© 2018. Published by The Company of Biologists Ltd | Journal of Cell Science (2018) 131, jcs210237. doi:10.1242/jcs.210237

RESEARCH ARTICLE

MARCKS-related protein regulates cytoskeletal organization at cell–cell and cell–substrate contacts in epithelial cells

Christina M. Van Itallie[1,*], Amber Jean Tietgens[1], Angel Aponte[2], Marjan Gucek[2], Alexander X. Cartagena-Rivera[3], Richard S. Chadwick[3] and James M. Anderson[1]

ABSTRACT

Treatment of epithelial cells with interferon-γ and TNF-α (IFN/TNF) results in increased paracellular permeability. To identify relevant proteins mediating barrier disruption, we performed proximity-dependent biotinylation (BioID) of occludin and found that tagging of MARCKS-related protein (MRP; also known as MARCKSL1) increased ∼20-fold following IFN/TNF administration. GFP–MRP was focused at the lateral cell membrane and its overexpression potentiated the physiological response of the tight junction barrier to cytokines. However, deletion of MRP did not abrogate the cytokine responses, suggesting that MRP is not required in the occludin-dependent IFN/TNF response. Instead, our results reveal a key role for MRP in epithelial cells in control of multiple actin-based structures, likely by regulation of integrin signaling. Changes in focal adhesion organization and basal actin stress fibers in MRP-knockout (KO) cells were reminiscent of those seen in FAK-KO cells. In addition, we found alterations in cell–cell interactions in MRP-KO cells associated with increased junctional tension, suggesting that MRP may play a role in focal adhesion-adherens junction cross talk. Together, our results are consistent with a key role for MRP in cytoskeletal organization of cell contacts in epithelial cells.

KEY WORDS: Marcksl1, MRP, Actin, Cell contact, Focal adhesion, Cytoskeleton

INTRODUCTION

Epithelial cells form polarized cell sheets that seal tissue spaces and allow the directional secretion and absorption of ions and solutes. This organization depends on the formation and maintenance of several types of intercellular contacts, namely tight, adherens and gap junctions and desmosomes, as well as on integrin-based adhesive interactions with the extracellular matrix (Hopkins et al., 2003; Koch and Nusrat, 2009). All of these junctions are connected to cytoskeletal elements, which provide structural integrity to the cell and also dynamically modulate and integrate intracellular forces to regulate many aspects of cell and monolayer behavior, including cell shape, differentiation, migration and polarity (reviewed in Mui et al., 2016).

[1]Laboratory of Tight Junction Structure and Function, National Institutes of Health, Building 50, Room 4525, 50 South Drive, Bethesda, MD 20892, USA. [2]Proteomics Core, National Heart, Lung and Blood Institute, National Institutes of Health, Building 50, Room 4525, 50 South Drive, Bethesda, MD 20892, USA. [3]Section on Auditory Mechanics, National Institute on Deafness and Other Communication Disorders, National Institutes of Health, Building 50, Room 4525, 50 South Drive, Bethesda, MD 20892, USA.

*Author for correspondence (Christina.vanitallie@nih.gov)

C.M.V., 0000-0003-1687-731X

Received 28 August 2017; Accepted 4 December 2017

MARCKS-related protein (MRP; also known as MARCKSL1) has been implicated in the coordination of membrane–cytoskeletal signaling events in non-epithelial cells, including integrin activation (Li et al., 1996), cell spreading (Yue et al., 2000), cell–cell adhesion (Finlayson and Freeman, 2009) and migration (Bjorkblom et al., 2012). MRP is a small myristoylated protein that contains a central region that binds calmodulin and is phosphorylated by protein kinase C (PKC) (Blackshear et al., 1992); MRP is also multiply phosphorylated by c-Jun N-terminal kinase (Bjorkblom et al., 2012) and likely numerous other kinase pathways (Hornbeck et al., 2012). It has been shown to localize to lateral cell membranes in MDCK cells in a PKC-dependent fashion (Myat et al., 1998), but there is little evidence that it has a role in integrin-dependent cytoskeletal structures and signaling in epithelial cells. MRP is structurally and functionally related to its better-studied relative, MARCKS, an actin crosslinking protein (Hartwig et al., 1992), but unlike MARCKS, a role for MRP in actin organization is unclear and may depend on phosphorylation state (Wohnsland et al., 2000; Bjorkblom et al., 2012).

Cytokine treatment of epithelial cells results in cytoskeletal reorganization at both cell–cell and cell–matrix interaction sites (Koukouritaki et al., 1999; Zolotarevsky et al., 2002; Hwang et al., 2012; Bianchi-Smiraglia et al., 2013) with much interest focused on their pathologic role in disrupting the intercellular tight junction barrier (Clayburgh et al., 2004). Administration of the pro-inflammatory cytokines, interferon-γ (IFN) and tumor necrosis factor-α (TNF) (hereafter INF/TNF) results in phosphorylation of the regulatory myosin light chain (MLC), which is thought to result in cytoskeletal contraction and is associated with increased paracellular flux of ions and solutes (Zolotarevsky et al., 2002). The increase in MLC phosphorylation also results in enhanced endocytosis of the tight junction protein, occludin (Marchiando et al., 2010). To identify proteins that were localized near to occludin (hereafter described as occludin proximal proteins) that might be associated with changes in endocytosis and barrier function following TNF and IFN treatment, we used occludin fused to a promiscuous biotin ligase (Roux et al., 2012; Fredriksson et al., 2015) expressed in MDCK cells with and without cytokine treatment. Unexpectedly, MRP was one of the most highly enriched occludin proximal proteins in cytokine-treated cells.

To better understand the role of MRP in epithelial cells, we deleted MRP from MDCK cells by using CRISPR/Cas9 methods and observed a wide range of phenotypes all consistent with loss of integrin activation, including decreased phospho-focal adhesion kinase (FAK; also known as PTK2) levels, alterations in the number and size of focal adhesions, and decreased cell spreading and migration. In addition, there was evidence for a coincident increase in cell–cell tension, cell height and accumulation of vinculin and a sarcomere-like α-actinin and myosin pattern at the apical junctional complex.

Journal of Cell Science (2018) 131, jcs210237. doi:10.1242/jcs.210237

RESULTS

Proinflammatory cytokine treatment of intestinal epithelial cells results in occludin internalization (Clayburgh et al., 2005). To test whether there were a similar response in MDCK cells, we treated MDCK cells with IFN and TNF and analyzed occludin localization with stimulated emission depletion (STED) microscopy (Hell, 2007). We found no appreciable change in ZO-1 (also known as TJP1) localization upon cytokine treatment (Fig. 1, all left panels), but, as previously seen in Caco-2 and T84 intestinal cells (Bruewer et al., 2003; Wang et al., 2005), there was a modest increase in intracellular occludin vesicles in cytokine-treated MDCK cells compared with controls (Fig. 1A). Line scanning across the tight junction region in two adjacent cells demonstrated a small increase in fluorescence signal away from the membrane in treated cells compared with controls (Fig. 1A, graph), consistent with this observation. We also found an increased concentration of actin, as detected with fluorescent phalloidin, around the junctional region (Fig. 1B) and a more dramatic increase in the accumulation of non-muscle myosin 2B (NMM2B) (Fig. 1C) after cytokine treatment.

Given the partial relocalization of occludin, actin and myosin following administration of IFN/TNF, we asked whether we could use BioID followed by mass spectrometry (MS) of biotinylated proteins to identify changes in occludin proximal proteins after cytokine treatment. To do this, we first tested the cytokine response of our previously described MDCK cell line stably expressing an inducible occludin tagged with a promiscuous biotin ligase (Fredriksson et al., 2015). We found induction of biotin ligase-fused occludin resulted in the same physiological responses we had previously described in MDCK cells expressing untagged occludin. Treatment with IFN/TNF resulted in both increased transepithelial electrical resistance (TER) and increased flux (Fig. 2A), and the increase in flux was exaggerated by occludin overexpression (Van Itallie et al., 2010). In control cells, following incubation with biotin, both biotin-ligase–occludin and fluorescent streptavidin, used to identify biotinylated proteins, concentrated at lateral cell contacts (Fig. 2B, top panels). A similar localization was found after cytokine treatment (Fig. 2B, bottom panels), but in this case, some large streptavidin and occludin-positive vesicles were also found in the cell cytoplasm (Fig. 2B, bottom panels, arrows).

MDCK cells induced to express biotin ligase-fused occludin were left untreated or treated with cytokines for 48 h; biotin was added to all cells for the final 16 h. Biotinylated proteins were purified, separated by SDS-PAGE, digested and extracted and peptides analyzed by MS as previously described (Fredriksson et al., 2015). Triplicate experiments were used to identify the most abundant occludin proximal proteins in control and cytokine-treated cells. Unexpectedly, one of the most enriched proteins identified was MRP; it was the third most abundant occludin proximal protein isolated from IFN/TNF-treated cells, but number 140 on the list of proteins from control cells (Fig. 2C; for full lists, see Tables S1 and S2).

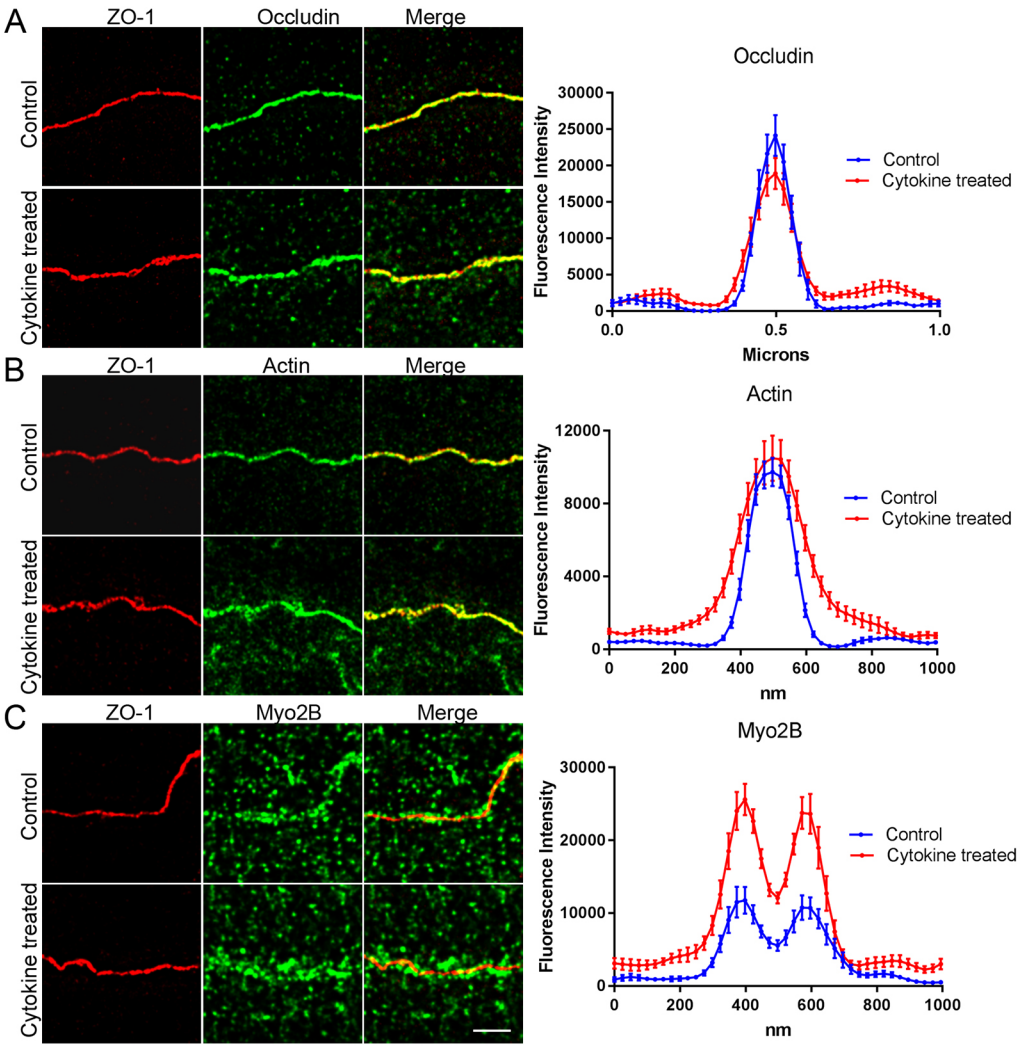

Fig. 1. STED microscopy reveals subtle differences in the localization of tight junction and cytoskeletal proteins after cytokine treatment. (A) Top left panels, colocalization of ZO-1 and occludin showing an increase in the cytoplasmic distribution of occludin after treatment with IFN/TNF. The graph represents line scans (n=16 for each protein) centered on the ZO-1 signal showing a small shift from junctional localization of occludin to vesicular signal (peak shoulders, red). (B) Left panels, colocalization of actin with ZO-1 showing close junctional colocalization in untreated cells that becomes more diffuse with cytokine treatment. The graph shows the increased spread of actin across junctional region after cytokine treatment. (C) Left panels, colocalization of myo2B (NMM2B) with actin showing that myo2B is normally associated with ZO-1 in peripheral region of the cell inside the tight junction; myo2B staining become stronger and spreads laterally after cytokine treatment. The line scans show that the myo2B signal is laterally displaced from the junctional region in control cells, and cytokine treatment results in increased junctional fluorescence as well as lateral spread of the fluorescent myo2B signal. Lines scans are mean±s.e.m. Scale bar: 1 µm.

Journal of Cell Science (2018) 131, jcs210237. doi:10.1242/jcs.210237

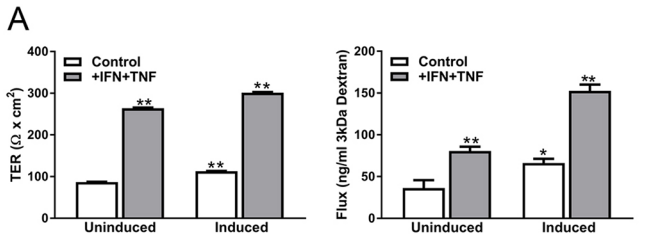

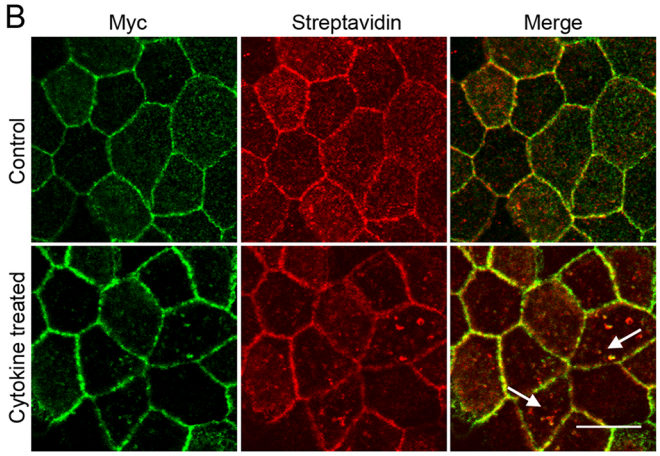

C

Cytokine List Position	Name	Control List Position
1	Occludin	1
2	Coxsackie and adenovirus receptor	16
3	MARCKS-related protein	140
4	Protein 4.1	5
5	Tight junction protein ZO-2	11
6	CD44	54
7	Rab11 family interacting protein 1	49
8	Charged multivesicular body protein 6	25
9	Gamma adducin	10
10	Catenin delta-1	9

Fig. 2. Proteomic analysis of cytokine-treated MDCK cells expressing occludin fused to biotin ligase results in identification of MRP. (A) MDCK cells stably expressing an inducible Myc–biotin-ligase–occludin were cultured with (uninduced) or without (induced) doxycycline and treated with IFN/TNF. Left panel, occludin overexpression results in a small increase in TER (20%), while cytokine treatment increased TER ~3-fold, with no difference in TER between cytokine-treated cells with and without occludin induction. Right panel, cytokine treatment results in increased paracellular flux that is potentiated by occludin overexpression. Results are mean±s.e.m., n=4 for all measurements, each experiment was repeated at least twice. *P<0.05; **P<0.001 (one-way ANOVA followed by Dunnett's multiple comparison test). (B) Immunofluorescence reveals colocalization of Myc-tagged biotin-ligase–occludin and biotinylated proximal proteins labeled by fluorescent streptavidin in untreated cells (top panels) and cytokine-treated cells (bottom panels). Increased colocalization of the vesicular Myc and streptavidin signal is evident in cytokine-treated cells, arrows, bottom right panel. Scale bar: 10 µm. (C) Enumeration of the most abundant occludin proximal proteins in the MS studies after cytokine treatment shows enrichment of MRP.

MRP has been previously reported to be modestly induced (less than 2-fold) upon TNF treatment of intestinal enteroids (Wood et al., 2016). We thus asked whether the observed enrichment of MRP tagging that we saw after cytokine treatment in MDCK cells was also due to induction of MRP expression. As determined by quantitative real-time PCR (qRT-PCR), we found that in MDCK cells, cytokine treatment resulted in a 20-fold induction of MRP mRNA expression (Fig. 3A, left); there was smaller but still significant increase in MRP mRNA expression in Caco-2 cells following cytokine treatment (Fig. 3A, right).

Despite significant effort, we were unable to identify a commercial antibody that recognized canine MRP in MDCK cells. We suspect that this is because the commercial antibodies are raised against synthetic human or mouse peptides and thus are less likely to recognize dog MRP, especially given that *in vivo* MRP is extensively and variably phosphorylated (Chang et al., 1996; Bjorkblom et al., 2012; Hornbeck et al., 2012). In addition, it seems likely that MDCK cells normally express low levels of MRP, since qRT-PCR results found that MRP mRNA was present at 5% of the level of ZO-1 mRNA in untreated cells. To determine cellular MRP localization, we instead stably expressed MRP tagged with GFP at the C-terminus in MDCK cells. Exogenous expression of MRP was verified by immunoblotting (Fig. 3B, left); as previously reported (Blackshear et al., 1992), although MRP is only 200 amino acids long (Blackshear et al., 1992; Tang and Brieher, 2012) and would be expected to migrate at ~23 kDa, it migrates anomalously as a ~40 kDa protein, or a 60 kDa+ protein with GFP tag in SDS PAGE gel electrophoresis. Expression of MRP–GFP had no effect on the levels of MDCK actin (Fig. 3B, left), occludin or E-cadherin (Fig. 3B, right). MRP–GFP partially colocalized with occludin in MDCK cells, but it was found all along the lateral membrane (Fig. 3C, top panels, arrow). This distribution has been previously described for MDCK cell MRP (Myat et al., 1998). More striking than the partial colocalization with occludin was the close colocalization with actin (Fig. 3C, lower panel). Colocalization was weak at the basal stress fibers (arrowhead), but strong at the lateral membrane (arrow).

Because MRP expression was increased in cytokine-treated cells, we asked whether overexpression of MRP altered the MDCK cell response to cytokines. As above, treatment with IFN/TNF resulted in increased TER (Fig. 3D) and increased flux (Fig. 3E) in wild-type (WT) MDCK cells. Expression of MRP GFP had no effect on basal TER or flux, but resulted in exaggerated increases in both TER and flux following IFN/TNF treatment (Fig. 3D,E); suggesting that MRP may, like occludin, be required for or modulate cytokine responses. MRP–GFP localization was more diffuse when cells were grown on semipermeable filters compared with when they were cultured on coverslips, but there was no obvious change in MRP–GFP localization with cytokine treatment (Fig. 3F).

To test whether MRP were required for cytokine response, we made CRISPR/Cas9-mediated MRP-knockout (KO) cell lines. Because we lacked an MRP antibody to verify knockout, we used a deletion strategy that would allow us to screen for potential KOs by PCR (Bauer et al., 2015). Two sets of primers for guide RNAs (Fig. 4A) were designed to flank a small intron within the MRP gene. These were separately cloned into CRISPR/Cas9 vectors and co-transfected into MDCK cells. The resulting clonal cell lines were then tested by genomic PCR for deletion of the region between the two sets of guide RNAs by using primers flanking the putative deletion (Fig. 4A). Results of PCR from WT and a representative MRP-KO cell line, showing the smaller PCR product, are shown in Fig. 4B. DNA from five putative KO cell lines was sequenced and all contained similar deletions of the region identified by the bracket in Fig. 4A.

To assess whether MRP KO resulted in changes in expression of junctional proteins, we compared expression of tight and adherens junction, and some cytoskeletal, proteins by immunoblotting and found no differences between WT and MRP-KO cell lines in occludin, NMM2B, E-cadherin, ZO-1, ZO-2 (TJP2) and vinculin (Fig. 4C). In addition, there were no obvious differences in the localization of tight or adherens junction proteins, as exemplified by occludin and E-cadherin immunolocalization (Fig. 4D). In no case did we see obvious changes in tricellular junctions (data not shown).

Journal of Cell Science (2018) 131, jcs210237. doi:10.1242/jcs.210237

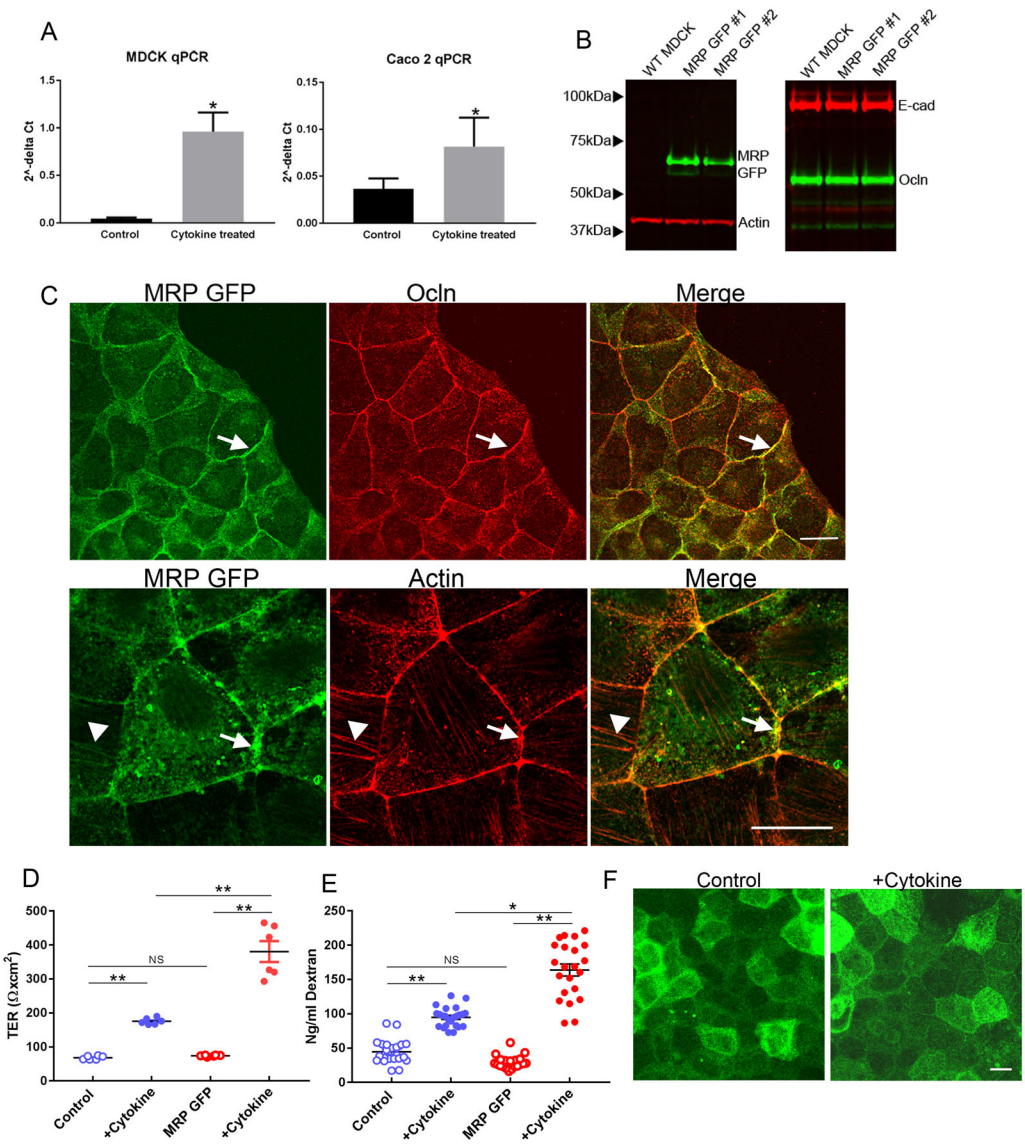

Fig. 3. MRP GFP predominantly colocalizes with lateral actin. (A) qRT-PCR of MDCK (right panel) and Caco-2 (left panel) cell RNA showing induction of MRP after cytokine treatment; amounts were normalized to ZO-1 mRNA levels in control and cytokine-treated cells. Results are mean±s.e.m., n=3 replicates; measurements repeated at least twice. *P<0.04 (unpaired t-tests). (B) Stable expression of MRP–GFP in MDCK cells did not alter levels of actin, E-cadherin or occludin. (C) Immunolocalization of MRP–GFP revealed some colocalization with apical occludin (top panels, arrows), but that MRP–GFP (and some occludin) was also localized to the lateral membrane. Colocalization was more evident with lateral actin (bottom panels, arrow), but there was also some weak colocalization at basal stress fibers (arrowhead) Scale bars: 10 µm. (D,E) Stable expression of MRP–GFP in MDCK cells potentiated the increase in TER (D, n=6) and flux (E, n=22 WT, N=24, MRP–GFP); three separately derived clones. Results are mean±s.e.m., *P<0.05; **P<0.001; NS, not significant (one-way ANOVA followed by Dunnett's multiple comparison tests) for indicated comparisons. (F) Cytokine treatment did not alter the distribution of MRP–GFP in MDCK cells. Scale bar: 5 µm.

We then asked whether MRP was required for the physiologic responses we observed after cytokine administration to MDCK cells. There was no obvious change in cytokine-induced occludin internalization in MRP-KO cells compared with controls (Fig. S1). Both basal and increased TER after cytokine treatment were observed in control and KO cell lines (Fig. 5A). However, paracellular dextran flux was considerably and equivalently (5–10-fold) increased in both untreated and treated MRP-KO cells compared with WT cells (Fig. 5B). These data do not suggest a requirement for MRP in the physiological response to cytokines, but instead indicate that MRP is critical in some way for normal monolayer integrity.

MRP has been implicated in both cell–cell (Myat et al., 1998) and cell–substrate attachment (Li et al., 1996), each of which might be expected to alter behavior observed in live-cell imaging. When confluent cultures of WT and MRP-KO MDCK cells grown on glass-bottomed dishes were imaged continuously for 12 h, both cell lines developed blisters in the monolayer, likely due to basal secretion of ions and fluid (Rabito et al., 1978). In WT cells, these blisters were small and resolved within a couple of hours (Fig. 5C, top panels; Movie 1). However, the blisters that formed in the MRP-KO layer were much larger and appeared to sequentially pull adjacent cells off the substrate as they grew (Rabito et al., 1980) (Fig. 5C, lower panels; Movie 2). The relative numbers (Fig. 5D) and sizes (Fig. 5E) of the blisters in the two cell lines were significantly larger in KO compared with WT cell lines.

Based on this observation and previous suggestions for a role for MRP in integrin-mediated substrate attachment in macrophages (Li et al., 1996), we compared the immunofluorescent localization of actin, and the focal adhesion and adherens junction protein vinculin, in KO and WT cells. Actin was concentrated at cell borders and less conspicuously in short basal stress fibers in WT cells (Fig. 6A, top left), while vinculin immunofluorescence was localized to small and numerous focal adhesions (Fig. 6A, top center). In contrast, actin (NMM2A and NMM2B staining are shown in Fig. S5) staining in MRP-KO cells revealed longer and more pronounced stress fiber staining that appeared to extend under adjacent cells (Fig. 6A, lower left), while focal adhesion staining for vinculin was much stronger and concentrated in large patches in KO compared with WT cells (Fig. 6A, lower center). Quantification of vinculin immunofluorescence revealed fewer (Fig. 6B) but larger (Fig. 6C) focal adhesions in the MRP KOs compared with MDCK WT cells. To determine whether these prominent focal adhesions could be rescued by re-expressing MRP, we transfected MRP KOs with

Journal of Cell Science (2018) 131, jcs210237. doi:10.1242/jcs.210237

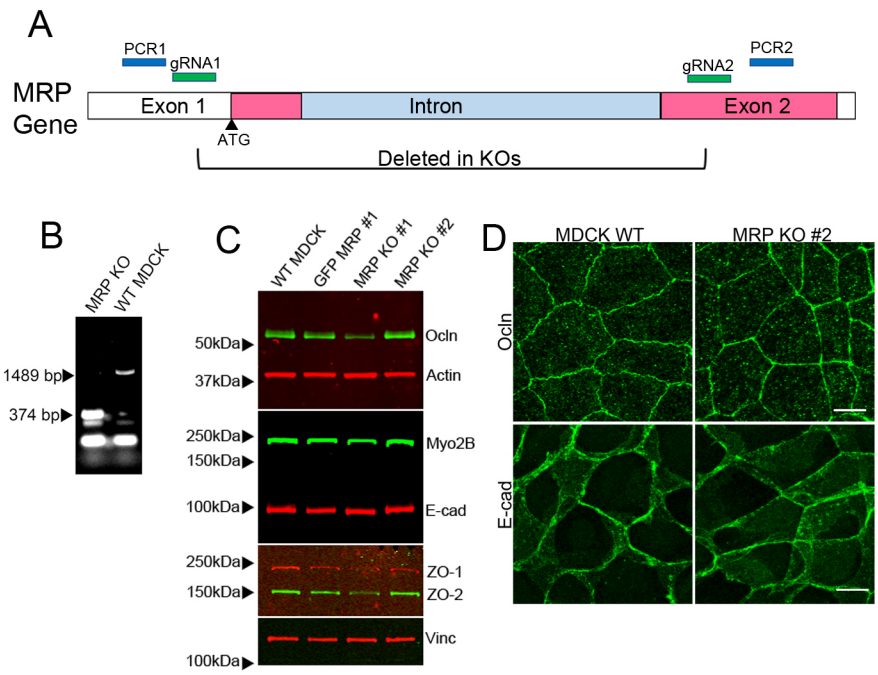

Fig. 4. MRP KO does not alter expression or localization of tight or adherens junction proteins. (A) Diagram of MRP deletion showing locations of sequences targeted by guide RNAs as well as flanking sequences used to design primers for PCR identification of mutant cell lines; bracket indicates deleted region confirmed by genomic sequencing. (B) PCR of genomic DNA from untransfected (right lane) and a cell line containing deletion as in A (left lane) showing PCR products used for identification of MRP-KO lines and sequencing. (C) Immunoblot analysis of WT, MRP–GFP-expressing and two MRP-KO cell lines reveals no consistent difference in expression levels of junction or cytoskeletal proteins. Myo2B, NMM2B. (D) Immunofluorescent analysis of control and KO cell lines showing no alteration in localization of occludin (top) or E-cadherin (bottom panels). Scale bars: 10 µm.

MRP–GFP and found diminished basal stress fiber formation and decreased focal adhesion size in GFP-expressing cells [Fig. 6D, compare expressing cells (*) with adjacent non-expressing KO cells]. This suggests that exogenous MRP can rescue this KO phenotype.

Overall, the actin and vinculin distribution across the monolayer was uniform in MDCK WT cells (Fig. 6E, top panels). However, although most of the MDCK KO monolayer showed increased focal adhesion staining as shown in Fig. 6A, there were occasional areas, delineated by a ring of concentrated actin (Fig. 6E, middle left panel, arrow, and enlarged, bottom left panel) that lacked these heavy stress fibers. Where diminished actin stress fibers were evident, there was also much reduced vinculin staining (Fig. 6E, middle and, enlarged, bottom center panels). It seems possible that these regions may represent areas that have either blistered or are prone to blistering (Fig. 5C).

To test directly whether, as in macrophages (Li et al., 1996), MRP is involved in cell spreading, we plated MDCK WT and KO cells on fibronectin for 4 h and measured cell size. Control but not KO cells spread well on fibronectin (Fig. 6F,H); this difference in spreading was rescued by expression of MRP–GFP in MRP-KO cells (Fig. 6G,H).

MRP has been implicated both in increased and decreased cell migration (Finlayson and Freeman, 2009; Bjorkblom et al., 2012), depending on phosphorylation state and cell context. Given the alterations in focal adhesion organization in the MRP KO, we tested the requirement for MRP in migration in a wound healing assay. At all times measured, there was a consistent delay in the migration of MRP-KO compared with MDCK WT cells (Fig. 6I).

FAK is a component of integrin-mediated signal transduction pathways; since MRP has been implicated in integrin activation pathways in macrophages (Li et al., 1996) and we observed that KO in MDCK cells resulted in altered focal adhesion morphology, we asked whether FAK localization or FAK phosphorylation were altered in MRP-KO cells. To test whether there were alterations in FAK distribution in MRP KOs, we co-immunostained WT and KO cells for FAK and ZO-1 (Fig. 7A). FAK localization in KO cells was similar to that of vinculin in both cell lines, confirming the altered size and number of focal adhesions in KO cells. Immunoblot analysis of FAK levels showed no change in total FAK, but a large decrease (15±7%, mean±s.e.m., of control levels) in phosphorylation of the major FAK autophosphorylation site, FAK(Y397); this was rescued by re-expression of MRP GFP (Fig. 7B). Levels of Src phosphorylated at Y416 [phospho-Src(Y416)], which is associated with FAK phosphorylation, were also modestly decreased in MRP-KO cell lines (50±15% of WT levels), although again, total Src levels were unchanged (Fig. 7B); actin and NMM2A levels were also unchanged between control, KO and rescue cell lines (Fig. 7B).

In addition to localization to the enlarged focal adhesions, FAK is also recruited to cell–cell contacts in KO but not WT cells (Fig. 7A, lower panels, arrow). Junctional FAK has been implicated in regulation of the stability of cell–cell adhesion (Han et al., 2013) and is required for tension-dependent assembly of the cadherin adhesion complex in *Xenopus* (Bjerke et al., 2014). Although MRP KO did not alter adhesion to E-cadherin (Fig. S6), we asked whether there were other indicators of increased tension at cell contacts and found in MRP KO cells increased actin and concentrated MLC phosphorylated at S19 [phospho-MLC(S19)] at cell contacts compared with WT cells (Fig. 7C, top, arrow). Even more dramatic was the accumulation of phospho-MLC(S19) at basal stress fibers (Fig. 7C); this locally increased phosphorylation is suggestive of both increased tension and decreased stress fiber turnover (Watanabe et al., 2007).

Given the recruitment of actin and phospho-MLC(S19) to cell contacts in MRP-KO cells, we asked whether α-actinin and vinculin were also recruited to cell contacts in KO cells. Tang and Brieher (Tang and Brieher, 2012; Kannan and Tang, 2015) have recently demonstrated that actin, vinculin and α-actinin-4 are recruited to adherens junctions upon the application of tension. We found, by immunofluorescence localization, that α-actinin and vinculin were increased at cell contacts in KO cells but this localization was barely detectable in controls (Fig. 7D). This change in distribution of tension-sensitive proteins suggested there might be an alteration in overall monolayer tension in the MRP-KO cells. To test this directly, we used noninvasive acoustic force microscopy (Cartagena-Rivera et al., 2017) to compare mechanical properties of WT and MRP-KO monolayers, and found increased tension in MRP-KO cells compared with WT MDCK cells (Fig. 7E).

Journal of Cell Science (2018) 131, jcs210237. doi:10.1242/jcs.210237

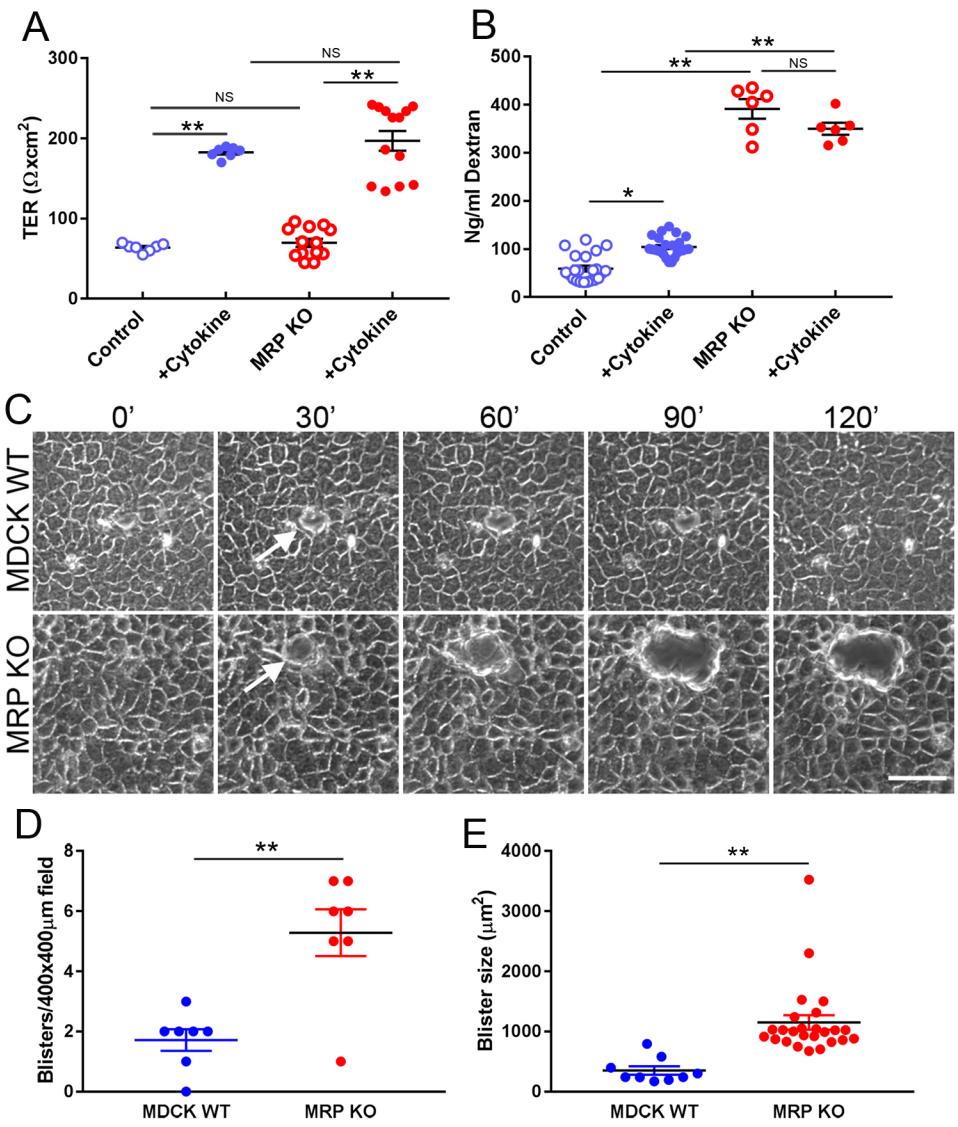

Fig. 5. Culture of MRP-KO cells on impermeant substrates results in monolayer blisters. (A) WT and MRP-KO (three separate clonal cell lines) cells show identical increases in TER. Results are mean±s.e.m., n=7 for controls; n=13 for KOs. in response to cytokine treatment. (B) MRP-KO cells show large increases in basal flux (8-fold over control values) that is not altered by cytokine treatment (n=24 for controls, n=6 for KOs. *P<0.05; **P<0.001; NS, not significant (one-way ANOVA followed by Dunnett's multiple comparison tests). (C) Time-lapse phase imaging of MDCK WT monolayer (upper panels) showing the appearance and resolution of small blisters over 2 h; in contrast, much larger blisters are evident in MRP-KO cell lines (bottom panels). Arrows highlight the blisters. Scale bar: 50 µm. (D,E) Quantification of the number of blisters (n=7) and blister size (n=9 for WT, n=25 for MRP KO) revealed that blisters are significantly more numerous and larger in MRP-KO cells compared with WT. Results are mean±s.e.m., **P<0.001 (unpaired t-tests).

Increased stress fibers and decreased focal adhesion turnover are consistent with increased Rho activity; however, we were unable to demonstrate increased active Rho (Fig. S2) nor could we reverse the actin stress fiber organization by administration of the cell permeant Rho inhibitor, C3 transferase (not shown). However, administration of the myosin ATPase inhibitor, blebbistatin (Fig. 7F), and to a lesser extent inhibition of Rho kinase (Fig. S3) resulted in equivalently disrupted stress fiber organization in both control and MRP-KO cells. However, neither inhibitor had an appreciable effect on the organization of lateral cell actin (Fig. 7F; Fig. S3).

Maintenance of cell shape in a monolayer depends on balanced tension around individual epithelial cells and across the monolayer (Choi et al., 2016); this tension is generated by the actin–myosin cytoskeleton. We noted that although the distribution of junctional NMM2B was fairly uniform across the monolayer in WT cells (Fig. 8A, left panel), whereas in the MRP-KO cells, NMM2B immunofluorescence was much more concentrated around some cells than others (Fig. 8A, right panel). MRP-KO cells had a more variable height distribution than WT cells (Fig. S4). This height variability was easily seen in scanning electron microscopic (SEM) analysis of the apical surfaces of MDCK WT and MRP-KO cells (Fig. 8B). The apical surface of MDCK WT cells was uniformly flat, while the MRP-KO cells had areas where the cells were humped up, suggesting that they were taller, which is consistent with increased, but irregular, junctional contraction.

To determine whether this imbalanced distribution of NMM2B was reflected in changes in the ability to maintain cell shape, we imaged confluent MDCK WT and MRP-KO monolayers over several hours. We found that, over 4 h, both WT MDCK and MRP-KO cells tended to maintain their position in a monolayer, but the geometric shape of WT cells remained relatively constant (Movie 3), while that of the MRP-KO cells was much more variable (Movie 4). The cell shape changes were quantified by measuring vertex–vertex distances in cells at 24 min intervals (Fig. 8C,D) over 4 h; the greater variability of the shape changes in MRP-KO compared with WT cells was reflected in the ranges observed (90.7–113% for WT, 69.5–175.4%) and coefficient of variation values for each (WT, 4.85%; KO, 22.36%).

DISCUSSION

Our studies identify MRP as a critical regulatory protein in the organization of epithelial cell–substrate and cell–cell contacts. Loss of MRP resulted in decreased cell migration, decreased spreading on fibronectin and the accumulation of several proteins that indicate

Journal of Cell Science (2018) 131, jcs210237. doi:10.1242/jcs.210237

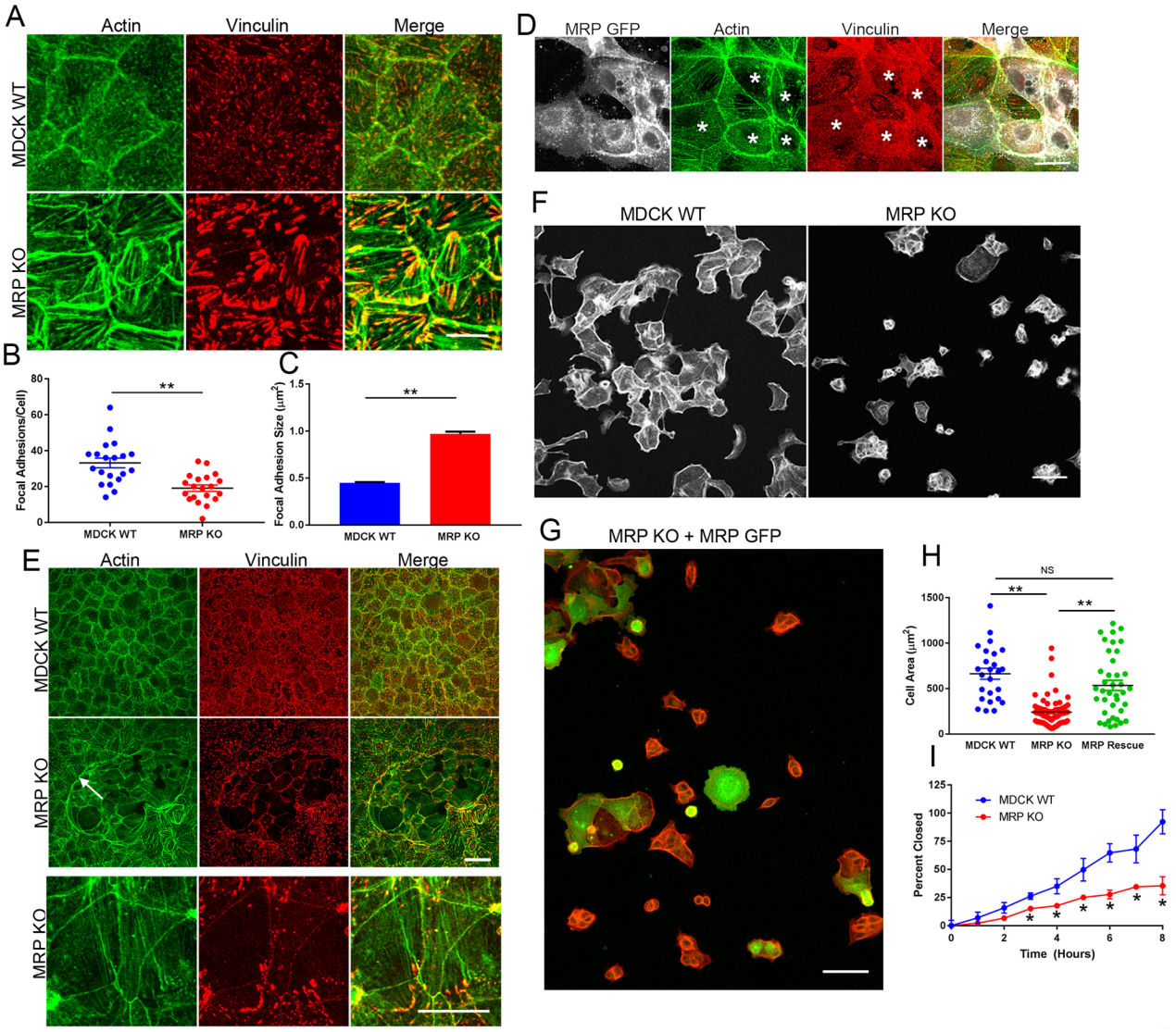

Fig. 6. MRP-KO cells have larger but fewer focal adhesions. (A) Maximum intensity projections of actin and vinculin immunofluorescence in WT (top panels) and MRP-KO (bottom panels) cells shows that actin stress fibers are much heavier in KO cells compared with controls, and vinculin staining of focal adhesions was much more pronounced in KO compared with WT cells. Scale bar: 5 µm. (B,C) Quantification revealed that there were fewer (B) but larger (C) focal adhesions in KO cells compared with WT cells (n=20). Results are mean±s.e.m., $^{**}P$<0.001 (unpaired t-test). (D) Transient transfection of MRP–GFP into KO cells resulted in decreased stress fibers and less-prominent focal adhesions in expressing cells (marked with *). Scale bar: 10 µm. (E) Low magnification images of WT (top panels) and KO cells (middle panels) showing patches within the monolayer delimited by a thick band of actin (arrow) with much reduced actin and vinculin staining; this is shown enlarged in the lower panels. Scale bar: 10 µm. (F) MRP-KO cells spread less well on fibronectin when compared to WT cells; cells were plated on fibronectin, allowed to attach and spread for 4 h and then stained for actin with Rhodamine–phalloidin. (G) The cell spreading defect in MRP-KO cells was rescued by transient transfection with MRP–GFP. Cells were plated, allowed to attach and stained for actin as above. Scale bar: 25 µm. (H) Cell spreading of WT, MRP-KO and MRP–GFP-rescued cells was quantified by measurement of cell area; there was no significant difference between sizes of WT and GFP-expressing cells, while MRP-KO cells were significantly smaller. Results are mean±s.e.m., n=25 (WT), 68 (KO), 38 (MRP GFP). $^{**}P$<0.001; NS, not significant (one-way ANOVA followed by Dunnett's multiple comparison tests). (I) Wound healing assay demonstrated slower migration in MRP-KO cells compared with WT cells. Results are mean±s.e.m., n=4; $^{*}P$<0.05 (paired t-test).

increased epithelial tension at both cell–substrate and cell–cell contacts, including phospho-MLC (Fanning et al., 2012), vinculin (Huveneers et al., 2012) and α-actinin (Tang and Brieher, 2012). Furthermore, MRP was required for cells to synchronize and balance tension among their multiple cell contacts resulting in uncoordinated changes in their polygonal shape. Despite the fact that MRP was identified in a BioID (Roux et al., 2012) protocol designed to find proteins involved in cytokine-dependent changes in paracellular permeability, KO of MRP did not reveal a specific role for MRP in tight junction regulation.

Although MRP has been primarily studied in the context of neural (Wu et al., 1996) and immune cells (Li and Aderem, 1992), it has also been previously found as a normal component of renal tubule cells (Huling et al., 2012). Our identification of MRP in cytokine-treated MDCK cells was likely primarily due to transcriptional induction of the protein, since MRP mRNA was present at low levels in untreated cells, but was increased 20-fold by combined treatment with IFN and TNF. This large induction of MRP was unexpected, since TNF treatment of enteroids results in less than a 2-fold induction of MRP (Wood et al., 2016), and neither

Journal of Cell Science (2018) 131, jcs210237. doi:10.1242/jcs.210237

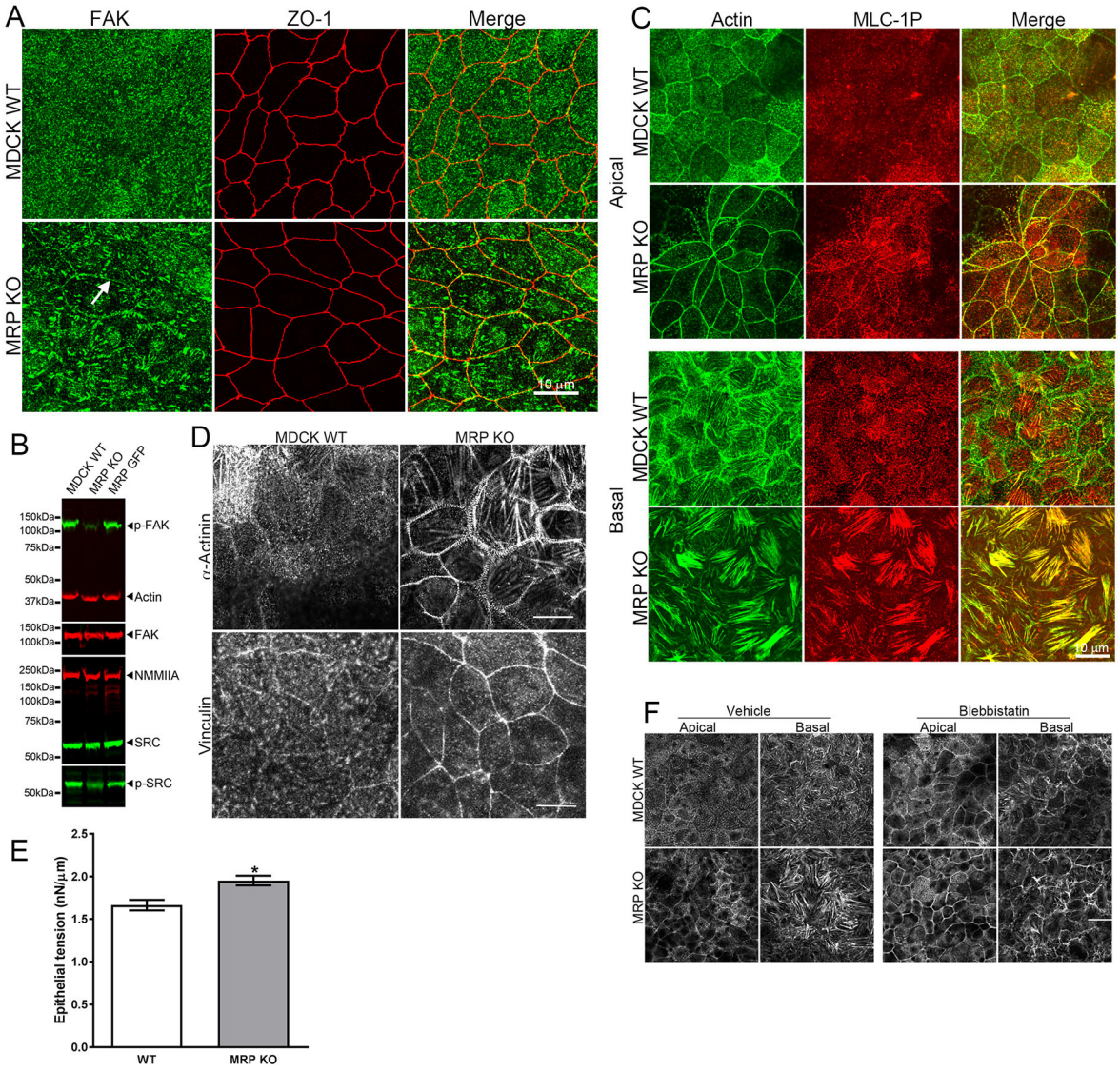

Fig. 7. MRP-KO cells have decreased phospho(Y397) FAK levels and increased phospho-MLC(S19) accumulation. (A) Maximum intensity projections of FAK and ZO-1 immunofluorescence in WT and MRP-KO cells showing larger and more sparsely distributed focal adhesion in MRP-KO cells and additionally, accumulation of FAK at cell–cell contacts only in KO cells (arrow). Scale bar: 10 µm. (B) Immunoblot analysis of WT, MRP-KO and MRP–GFP-expressing cells reveals that levels of phospho(Y397) FAK [p-FAK; 1±0.1 in WT, 0.13±0.04 in KO and 0.7±0.1 in MRP–GFP-expressing cells compared with controls, mean±s.e.m., n=3; P<0.05 (one-way ANOVA followed by Dunnett's multiple comparison tests)] and phospho-Src [p-SRC; 1±0.1 in WT, 0.5±0.1 in KO and 0.9±0.1 in MRP–GFP-expressing cells compared with controls, mean±s.e.m., n=3; P<0.05 (one-way ANOVA followed by Dunnett's multiple comparison tests)] were decreased in KO cells without changes in the expression levels of total FAK or Src. The expression levels of the other proteins were unchanged. (C) Immunolocalization of phospho(Ser19)-MLC (MLC-1P) revealed accumulation at cell–cell contacts in MRP-KO but not WT cells (top panels, arrow) and more association with basal stress fibers in KO cells compared with WT (bottom panels). Scale bar: 10 µm. (D) Immunofluorescence localization of α-actinin (top) and vinculin (bottom) in WT and MRP-KO cells revealing much heavier junctional accumulation in KO cells. Scale bar: 10 µm. (E) Acoustic force spectroscopy was used to measure monolayer tension in MDCK WT and MRP-KO cells; KO cells showed significantly increased tension (1.95±0.06 pN/µm, n=25) compared with WT cells (1.66±0.06 pN/µm, mean±s.e.m., n=28), *P=0.0013 (unpaired Student's t-test with Welch's correction). (F) Immunofluorescence localization of actin in MDCK WT and KO cells after treatment with blebbistatin (100 µM, 4 h) disrupts basal actin stress fiber organization in both WT and KO cells but not junctional actin accumulation. Scale bar: 20 µm.

TNF nor IFN induce MRP in microglial cells (Rosé et al., 1996; Murphy et al., 2003). MRP is dramatically induced by lipopolysaccharide (LPS) in microglial cells and in these cells, MRP depletion by means of siRNA results in decreased chemotaxis (Chun et al., 2009). However, the physiological importance of cytokine-stimulated MRP induction in MDCK cells is unclear, since although overexpression of MRP resulted in increased cytokine responsiveness, this may be due to a disruption of normal cytoskeletal interactions. In contrast, MRP KO did not suppress the response to TNF and IFN administration. Thus, unlike occludin (Marchiando et al., 2010; Van Itallie et al., 2010), MRP does not appear to be an obligatory component in cytokine-induced barrier loss.

MRP KO did reveal a number of striking phenotypes suggesting that the protein is normally critically involved in the regulation of cell–substrate and cell–cell interactions. MRP has previously been implicated in integrin-dependent cell signal transduction pathways (Li et al., 1996; Zhou and Li, 2000). Consistent with this idea, among the most dramatic findings in the MRP KOs were the increased size and decreased number of focal adhesions, and the

Journal of Cell Science (2018) 131, jcs210237. doi:10.1242/jcs.210237

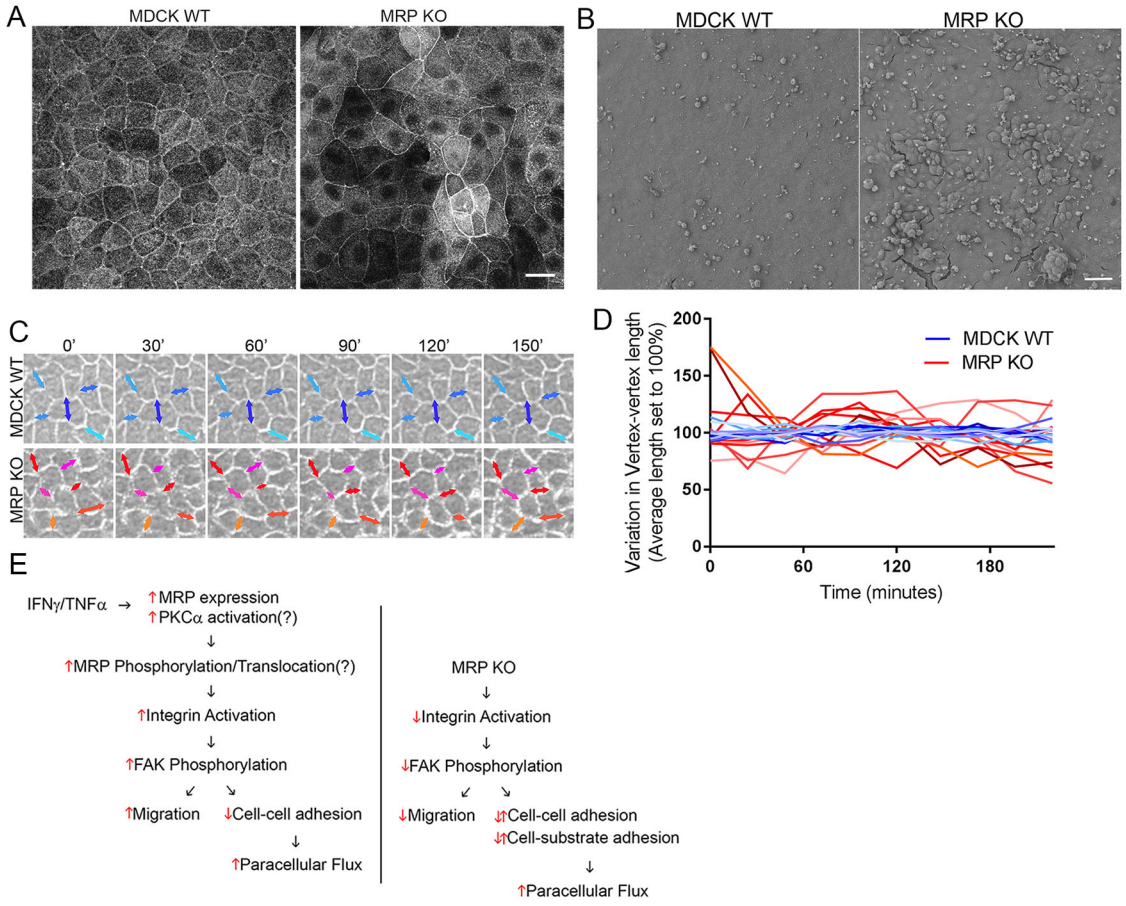

Fig. 8. MRP KO cells show evidence for unbalanced monolayer tension. (A) Immunofluorescence localization showing that apical/junctional Myo2B is uniform across WT monolayers but shows variable accumulation at cell contacts in MRP-KO cells. Scale bar: 10 µm. (B) SEM imaging of MDCK WT and MRP-KO cells reveals WT cells appear uniformly even, while the MRP KO monolayer is uneven, with areas of humped cells. Scale bar: 20 µm. (C) WT and KO cells were imaged every 30 min for 150 min; measurement of the lengths of individual bicellular contacts revealed little size length change in WT (top panels, examples shown with blue arrows) but much greater cell shape changes in MRP-KO cells (bottom panels, red arrows). *n*=10 WT and MRP KO. (D) Variation from the average bicellular length for any given bicellular contact is greater for MRP KO cells (red lines) compared with WT cells (blue lines) over the 4 h measurement period. (E) Speculative diagram of possible signaling pathways in cytokine treated and MRP-KO cells. For details, see the Discussion.

formation of very prominent basal actin stress fibers relative to WT cells. KO of FAK, which normally transduces integrin-dependent signaling (Schober et al., 2007), results in similar changes in focal adhesion number and size and in basal stress fiber organization, and these changes have been associated with diminished focal adhesion remodeling. FAK autophosphorylates in response to integrin signaling (Schaller et al., 1994); the loss of FAK phosphorylation in MRP-KO cells suggests that MRP is required upstream of FAK activation. Further evidence for the involvement of MRP in the integrin–FAK signaling pathway is the observed decrease in phospho-Src(Y416) levels, which is also seen in FAK-KO cells (Schober et al., 2007).

We speculate that the loss of FAK phosphorylation in MRP-KO cells might diminish the ability of focal adhesions to remodel and accommodate to the normal basal accumulation of fluid that accompanies polarized Na^+/K^+ ATPase activity (Leighton et al., 1969). It seems likely that loss of remodeling ability, possibly in conjunction with increased cell–cell tension (see below), might result in the formation of the large blisters that we observed in MRP-KO but not WT cells. Blister formation could also explain why occasional sites in the monolayer have lost most focal contacts.

We also observed that although MRP KO cells attached to fibronectin to the same degree as WT cells (Fig. S5), KO cells spread more slowly on fibronectin; this difference was rescued by MRP re-expression. This finding is consistent with previous studies that demonstrated a role for MRP in cell spreading (Li et al., 1996; Yue et al., 2000). In contrast, a more recent study has demonstrated that macrophages from MRP-KO mice spread normally on glass, (Underhill et al., 1998), suggesting the MRP is not essential for macrophage spreading. However, in this latter study (Underhill et al., 1998) spreading was only assessed after 24 h and thus did not rule out a facilitating role for MRP in initial stages of cell spreading; the differences we report were seen within 4 h after plating cells. In addition to the defect in cell spreading, we also noted that MRP-KO cells migrated more slowly than WT cells. Although a number of studies have demonstrated both stimulatory and inhibitory roles for MRP in cell migration, in some cases dependent on site-specific MRP phosphorylation, the consensus is that, as we found, MRP depletion is associated with decreased migration (Chun et al., 2009; Finlayson and Freeman, 2009; Bjorkblom et al., 2012; Kim et al., 2016). Although the mechanism causing the decreased migration is unclear, delayed migration is also seen in FAK-KO cells, where it is also thought to be related to defective focal adhesion remodeling (Schober et al., 2007).

Another similarity between the MRP- and FAK-KO cells is increased phospho-MLC seen on the basal stress fibers (Schober

et al., 2007) and the return of the basal stress fiber organization upon both myosin ATPase and ROCK inhibition (Schober et al., 2007).

FAK knockdown is associated with increased endothelial cell barrier function (Jean et al., 2014) and an increased strength of E-cadherin-dependent adhesion (Canel et al., 2010). Although we saw no evidence for changes in cadherin-dependent adhesion in MRP-KO cells (Fig. S5), direct measurement revealed increased monolayer tension in KO cells compared with WT controls. However, the distribution of phospho-MLC and the increased junctional localization for NMM2B, vinculin and α-actinin were not uniform across the MRP monolayer, nor was cell height. In addition, we found that MRP-KO cells were unable to maintain their shape as well as control cells; this could reflect unbalanced tension and/or might be related to the MRP–FAK pathway, since FAK-KO cells show increased nonproductive ruffling (Swaminathan et al., 2016).

Much recent data has suggested the existence of crosstalk between focal adhesions and cell–cell contacts (reviewed in Mui et al., 2016). Our results suggest a role for MRP in regulation of this cross-talk, but the lack of available antibodies and the presence of multiple sites for phosphorylation and other post-translation modifications on MRP means confidently assigning to a specific role or pathway in this process is difficult. The exact regulatory pathways relevant to MRP action in epithelial cells are unclear, but one speculative model outlining possible signaling pathways in cytokine-treated and MRP-KO cells is diagrammed in Fig. 8E. Many of these interactions are based on previously published studies (Lipfert et al., 1992; Cary et al., 1996; Myat et al., 1998; Zhou and Li, 2000; Chang and Tepperman, 2001; Ivey et al., 2009; Lie et al., 2012) and have not been validated by direct experimental analysis in epithelial cells. A better understanding of how MRP interacts with integrins in epithelia is a critical missing component in understanding coordination between cell–cell and cell–substrate interaction in adherent cells.

MATERIALS AND METHODS

Antibodies and reagents

Rat anti-ZO-1 [40.76, used at 1:500 for immunoblots (IB) and 1:100 for immunofluorescence, IF] has been previously described (Anderson et al., 1988), rabbit anti-occludin polyclonal antibody was from ProteinTech (13409-1-AP; 1:1000 IB, 1:800 IF), rabbit anti-ZO-2 (38-9100; 1:1000 IB, 1:100, IF) and anti-phospho-FAK(Tyr397) (700255; 1:1000 IB) antibodies were from ThermoFisher; mouse anti-FAK (610087; 1:1000 IB, 1:100 IF) and mouse anti-E-cadherin (61081)(1:1000 IB, 1:100 IF) antibodies were from BD Transduction Laboratories, rabbit anti-phospho-MLC(S19) (3671P; 1:100 IF), -Src (2109; 1:1000 IB), -phospho-Src(Tyr416) (2101;1:1000 IB) and mouse anti-Myc tag (9B11; 1:100 IF) antibodies were from Cell Signaling Technology; rat anti-E-cadherin (U3254; 1:200 IF), mouse anti-α-actinin (1:100 IF), mouse anti-γ-tubulin (1:1000 IB) and mouse anti-vinculin (V9131; 1:1000 IB, 1:100 IF) were from were from Sigma-Aldrich; rabbit anti-myosin 2B (909901) and 2A (909801) (1:1000 IF, 1:250 IB) antibodies were from BioLegend; rabbit anti-GFP antibody (Ab290); 1:2000 IB) was from Abcam; mouse anti-actin antibody (MAB1501R; 1:2000 IF) was from Millipore; mouse monoclonal antibody to GP135/podocalyxin (1:100 IF) was kindly provided by George Ojakian, State University of New York, NY. Antibodies were validated by recognizing bands of the predicted size on immunoblots and by immunolocalization where reported. Species-specific secondary antibodies for immunofluorescence [Cy2 (1:200), Cy3 (1:2000) and Cy5 (1:200) conjugated, Alexa Fluor 594-conjugated Affinipure F(ab′) Fragment IgG (1:200) and Alexa Fluor 647-conjugated Affipure F(ab′) Fragment IgG (1:200)] and immunoblots (IR-labeled 680 and 790/800 antibodies, all 1:2000) were from Jackson ImmunoResearch; fluorescent streptavidin (568; 1:800, IF) and Rhodamine–phalloidin (1:40) were from ThermoFisher.

(–)-Blebbistatin was from Sigma-Aldrich, Y-27632 was from Millipore, IFN-γ, TNF-α and E-cadherin FC chimera were from R&D Systems, Fibronectin was from ThermoFisher. Cell tracer Green CMFDA or Red CMPTX were from Molecular Probes, ThermoFisher.

The MRP–GFP construct was a generous gift from Eleanor Coffey, Turku Center for Biotechnology, Turku, Finland.

Cell culture and transfection

Tet-off MDCK II cells (BD Biosciences) were cultured in DMEM (4.5 g/l glucose), 10% fetal bovine serum, and penicillin-streptomycin. The cell line stably expressing Myc–biotin-ligase–occludin has been previously described (Fredriksson et al., 2015). Caco-2 cells (ATCC) were cultured in DMEM (4.5 g/l glucose), 10% fetal bovine serum (Atlanta Biologicals, Tet-tested), and penicillin-streptomycin supplemented with 1× non-essential amino acids and 10 mM HEPES (Corning). Unless otherwise described, WT and MRP-KO cells were cultured for 6–10 days before experiments.

Stable knockout clones were made using the CRISPR-Cas9 system (Ran et al., 2013) as modified by Bauer et al. for gene deletion (Bauer et al., 2015); two separate vectors targeting either side of intron 1 were designed (caccATAGTTCGGCCGGGTCGGCC and caccTGGCTCGATGGCATC-GCCAG; lowercase letters indicate nucleotides added for cloning). Oligonucleotides were phosphorylated, annealed and cloned into the *Bbs*I site of pSpCas9(BB)-2A-Puro vector (62988; Addgene; deposited by Feng Zhang; Ran et al., 2013) according to the Zhang laboratory protocols (Feng Zhang, MIT, Cambridge, MA). All constructs were verified by sequencing.

MRP–GFP (Bjorkblom et al., 2012) and CRISPR/Cas9 constructs were transfected into MDCK II Tet-off cells by using Lipofectamine 2000. To make stable lines, MRP–GFP was co-transfected with pSVZeo (ThermoFisher) into both WT and MRP-KO cell lines and selected with 1 mg/ml zeocin (InvivoGen); individual clones were selected and expression verified by immunoblotting with anti-GFP antibody; three MRP–GFP-expressing lines and one rescue line were used for further analyses. In some cases, MRP–GFP was transiently transfected into KO cell lines by using Lipofectamine; cells were analyzed 48 h after transfection. To make KO cell lines, cells were co-transfected with pBlast49 (InvivoGen), and 10 µg/ml blastocidin (InvivoGen) was added 16 h after transfection. Cells were selected for 24 h and then single cells isolated by dilution cloning into 96-well plates. Individual clones were tested by PCR of genomic DNA (DNeasy kit, Qiagen) and MRP deletions identified by PCR using primers upstream and downstream of the putative deletion site (5′-GCAT-TCTGGCGCGGAGCGGAG-3′ and 5′-ATTCTGCTCGCCGGCAGGTG-3′). MRP KOs from four separately derived cell clones were verified by sequencing of PCR products; deletions for all four were in the expected region between the two guide RNA sites.

Assays of paracellular barrier function

TER (WPI) and flux assays were carried out as previously described (Van Itallie et al., 2010) by using fluorescein-labeled 3-kDa dextran (ThermoFisher). All measurements are performed in triplicate and replicate experiments were performed at least three times. Barrier function assays performed with MRP-KO and MRP–GFP-expressing cells were performed with at least three separately derived clonal cell lines.

Immunoblots and RhoA-GTP binding assay

For immunoblots, cells were plated on 35 mm dishes or 12 mm Transwell filters (Corning) and grown for 7–10 days. Cells were washed twice in ice-cold Dulbecco's phosphate-buffered saline (Corning) and lysed in 0.15–0.25 ml of 4× SDS sample buffer (250 mM Tris-HCl pH 6.8, 40% glycerol, 0.57 M 0.3 M β-mercaptoethanol and 8% SDS). Lysates were sonicated briefly to shear genomic DNA, heated to 95°C for 3 min, and resolved by SDS-PAGE. Gels were transferred to nitrocellulose filters and then blocked in a solution of PBS and 10% non-fat dry milk powder (NFDM) for 1 h. Filters were incubated for 1 h in primary antibodies diluted in a solution of PBS, 5% NFDM and 0.1% Tween-20 (PBS-T); washed four times for 5 min each in PBS-T; and incubated for 30 min with 1:2000 dilution of the appropriate species-specific secondary antibodies coupled to IRDyes (Rockland, Gilbertsville, MD). After four more washes in PBS-T, filters were imaged with the Odyssey infrared imaging system (Licor Biosciences, Lincoln, NE).

Active Rho was assessed by using the RhoA pulldown activation assay kit (Cytoskeleton) according to the manufacturer's instructions.

All immunoblot experiments were performed at least twice.

Immunofluorescence microscopy

MDCK cells were cultured on uncoated glass coverslips or on Transwell filters (Corning), fixed in ice-cold ethanol at 4°C for 30 min or in 1–4% paraformaldehyde in CSK buffer (10 mM 1,4-piperazinediethanesulfonic acid, pH 6.8, 100 mM KCl, 300 mM sucrose, 2 mM $MgCl_2$, and 2 mM ethylene glycol tetraacetic acid) at room temperature for 20 min, permeabilized with 1% Triton X-100 for 10 min, quenched with 50 mM NH_4Cl, and incubated in 2% normal goat serum in phosphate-buffered saline (PBS) for 60 min and in primary antibodies for 60 min. After washing, samples were incubated with fluorescence-labeled secondary antibodies; in some cases Rhodamine- or Alexa Fluor 647-conjugated phalloidin was added with the secondary antibodies. After washing, samples were mounted with Mowiol containing 1% *n*-propyl gallate.

Fluorescence imaging was performed with a Zeiss (Thornwood, NY) 710 confocal microscope, using a 63×/NA 1.4 oil objective or 20× air objective, with 488-, 561- and 633-nm laser lines, or a Zeiss LSM 880 Airyscan in Super resolution mode with a 63×1.4 NA objective. Raw data were processed using Airyscan processing with 'auto strength' (mean strength± s.d.=5.5±1.3) in Zen Black software version 2.3. Time-lapse phase imaging was performed on cells plated on two- or four-chamber Lab-Tek glass bottom dishes and imaged using a Nikon Eclipse Ti (Nikon Instruments) with a 20×0.45 NA objective phase lens and heated stage; images were acquired using Nikon NIS Elements software.

All immunofluorescence imaging was performed multiple times on several MRP-KO, MRP–GFP-expressing and rescue cell lines.

Stimulation emission depletion super resolution microscopy

MDCK cells were cultured for 6 days on transwell filters (Corning, Pittson, PA), and then treated or not for 48 h with 100 ng/ml IFN and 30 ng/ml fixed and stained as described in the above section, STED images were obtained by using a commercial Leica SP8 STED 3X system (Leica Microsystems, Mannheim, Germany), equipped with a white light excitation laser and the depletion lasers (592, 660 and 775 nm). A 100×/1.4 NA oil immersion objective lens (HCX PL APO STED white, Leica Microsystems) was used for imaging. Image stacks were collected as 8-bit, 1024×1024 pixels images with 25 nm *x* and *y* pixel sizes, six line averages, frame accumulation=2 and 0.2 µm *z*-steps. Rat anti-ZO-1 monoclonal antibody and anti-NMM2B primary, with secondary Alexa Fluor 594-conjugated F(ab′) fragment IgG and Rhodamine–phalloidin were imaged at 594 nm (775 STED depletion laser set at 20% power), and rat anti-ZO-1 with Alexa Fluor 647-conjugated F(ab′) Fragment IgG secondary antibody at 647 nm (775 nm STED depletion laser set at 5% power); time gating was set to 0.7 ns. STED image stacks were deconvolved using Huygens software (Scientific Volume Imaging B.V., Hilversum, The Netherlands), and stacks edited using Fiji image analysis software to make maximum intensity *Z*-projections of the top five out of nine images (1.1 µm *z*-axis dimension) and final images were assembled in Adobe Illustrator 10 (Adobe Systems Incorporated) software. All settings for control and KO cell lines were matched; 647 images are shown as red and 594 as green. Line scanning was performed with ImageJ (NIH); 13–18 line scans for each antigen/condition were used to generate graphs.

Purification of biotinylated proteins for mass spectrometry

MDCK II Tet-off cells inducibly expressing Myc–biotin-ligase–occludin (Fredriksson et al., 2015) were cultured in absence of doxycycline for 6 days in 75-mm transwell inserts (Corning) and then treated or not for 48 h with 100 ng/ml IFN and 30 ng/ml TNF; 50 µM biotin (Millipore Sigma, Billerica, MA) was added for the final 16 h. For each proteomic analysis, cells from six filters were combined. Affinity capture of biotinylated proteins was performed as described previously (Van Itallie et al., 2013) with slight modifications; cells were washed in PBS twice, scraped in PBS, pelleted and lysed in 1.5 ml of radioimmune precipitation buffer (1% Triton X-100, 0.5% deoxycholate, 0.1% SDS, 50 mM Tris-HCl pH 7.5, 150 mM NaCl supplemented with protease inhibitors). Samples were sonicated, incubated on ice for 20 min, resonicated, and centrifuged for 20 min at 12,000 ***g*** to remove insoluble material. Supernatants were transferred to fresh tubes containing 50 µl of (slurry) prewashed Dynabeads MyOne Streptavidin C1 and incubated for 2 h at 4°C in an end-over-end mixer. Beads were washed for 8 min twice with 2% SDS; once with 0.1% deoxycholate, 1% Triton X-100, 500 mM NaCl, 1 mM EDTA, 50 mM Hepes, pH 7.3, and once with 250 mM LiCl, 1 mM EDTA, 0.5% deoxycholate, 0.5% Nonidet P-40, 10 mM Tris-HCl pH 8.0, followed by two washes in 50 mM Tris-HCl pH 7.5, 50 mM NaCl at room temperature. Bound proteins were eluted by a 10-min incubation at 96°C in biotin-saturated 4× SDS sample buffer (8% SDS, 250 mM Tris, pH 6.8, 0.57 m mercaptoethanol, 40% glycerol). Eluted proteins were subjected to SDS-PAGE, and gels were stained briefly with SimplyBlue Safe Stain (Invitrogen). Lanes were excised and divided into 12–16 bands, then destained, reduced, alkylated and digested overnight with trypsin (Promega, V511A Sequencing grade). Eluted peptides were purified on ZipTips (C18, Millipore) and transferred into sample vials (Agilent, Santa Clara, CA) for mass spectrometry.

Mass spectrometry, database search and data analysis

All mass spectrometry experiments were performed in replicates on an Orbitrap Fusion coupled with an Ultimate 3000-nLC (Thermo Fisher Scientific). Peptides were separated on a EASY-Spray C_{18} column (Thermo Fisher Scientific; 75 µm×25 cm inner diameter, 2 µm particle size and 100 Å pore size). Separation was achieved by 5–35% linear gradient of acetonitrile +0.1% formic acid over 120 min. An electrospray voltage of 2.1 kV was applied to the eluent via the EASY-Spray column electrode. The Orbitrap Fusion was operated in positive ion data-dependent mode. Full scan MS^1 was performed in the Orbitrap with a normal precursor mass range of 350–1500 *m/z* at a resolution of 120 k. The automatic gain control (AGC) target and maximum accumulation time settings were set to 4×10^5 and 50 ms, respectively. MS^2 was triggered by selecting the most intense precursor ions above an intensity threshold of 5×10^3 for collision-induced dissociation (CID)-MS^2 fragmentation with an AGC target and maximum accumulation time settings of 5×10^2 and 250 ms, respectively. Mass filtering was performed by the quadrupole with a 1.6 *m/z* transmission window, followed by CID fragmentation in the ion trap (rapid mode) and a normalized collision energy (NCE) of 35%. To improve the spectral acquisition rate, parallelizable time was activated. The number of MS^2 spectra acquired between full scans was restricted to a duty cycle of 3 s.

Raw data files were processed using Proteome Discoverer (v1.4, Thermo Fisher Scientific), using the Mascot v2.5.1 (Matrix Sciences) search node. All searches were performed against the protein database NCBI non-redundant (NCBInr_20160823), with, for taxonomy *Canis lupus familiaris* (dog). Search modifications used were as follows; (fixed) carbamidomethyl of cysteine, (variable) oxidation of methionine, deamidation (NQ) and acetyl on protein N-terminus. For MS^2, the precursor and fragment ion tolerances of 12 ppm and 0.6 Da were applied, respectively. Up to two-missed tryptic cleavages were permitted. Target Decoy was used to calculate the false discovery rate (FDR) of peptide spectrum matches, set to a *P*-value of 0.05 (Elias and Gygi, 2010).

Protein samples were analyzed by MS in triplicate from three independent experiments. Inclusion in the final list required identification in two of the three experiments; after the list was compiled, keratins, histones and carboxylases were discarded. The total peptide spectrum match (PSM) for each individual experiment was calculated and used to derive normalized PSM values; the average normalized PSM/observable peptide number was then calculated as previously described (Van Itallie et al., 2014). All proteins that were enriched by less than three times over the biotin ligase alone were discarded (Fredriksson et al., 2015) and the remaining proteins ranked by average normalized PSM/observable peptide number.

Quantitative real-time PCR

MDCK II tet-off cells were cultured for 6 days on 24 mm Transwell filters (Corning) and then treated with 30 ng/ml TNF and 100 ng/ml IFN for 48 h. RNA was using the RNeasy minikit (Qiagen, Germantown, MD). 1000 ng of RNA was used for cDNA synthesis with the Superscript VILO Master Mix (Life Technologies). cDNAs were diluted 1:10 and amplified by using the Power Sybr Green Master Mix (Life Technologies). Primers for qRT-PCR are as described below. qRT-PCR was performed using LightCycler

96 thermocycler (Roche, Basel, Switzerland). qRT-PCR measurements were performed in triplicate and performed three times. The following primers were used for qRT-PCR: human ZO-1, 5′-CTGGTGAAATCCC-GGAAAAATGA-3′ and 5′-TTGCTGCCAAACTATCTTGTGA-3′, canine ZO-1, 5′-AGTTTGTCTCCACGGTCTGA-3′ and 5′-GGATTTCACCAA-TGTGACTT-3′; human/canine MRP, 5′-ATGGGCAGCCAGAGCTCC-AAGGCT-3′ and 5′-CCATTGCTTTTCACGTGGCCATTC-3′.

Scanning electron microscopy

Cells were grown for 10 days on 12×12 mm coverslips, then directly fixed in 2.5% glutaraldehyde and 1% paraformaldehyde in 0.12 M sodium cacodylate buffer, pH 7.4, for 20 min at room temperature and 40 min at 4°C. Cells were post-fixed with 1% osmium tetroxide, stained with uranyl acetate, ethanol dehydrated, and dried using a Samdri-795 critical point dryer (Tousimis Research Corp, Rockville, MD). Samples were mounted on carbon adhesive stubs and sputter coated with 5 nm of gold by using the EMS 575-X sputter coater (Electron Microscopy Sciences, Hatfield, PA). Images were captured on a Zeiss Crossbeam 540 SEM (Carl Zeiss Microscopy LLC, Thornwood, NY).

Cell attachment, spreading assay, height, migration, blister and focal adhesion measurements

The cell attachment assay was performed as previously described (Van Itallie et al., 2014), except that cells were allowed to adhere for 2 h and fluorescence was read using a plate reader (Spectramax M3, Molecular Devices, using SoftMax Pro 5.4 software); the attachment assay was performed twice.

Cell spreading was assessed by coating glass coverslips (12 mm, round) with 10 µg/ml fibronectin at 37°C for 45 min; WT, KO and rescue cells were plated at 7.5×10^4 cells/well and allowed to attach and spread for 4 h. Cells were fixed with 4% paraformaldehyde and actin stained with Rhodamine–phalloidin. Cell size was assessed after thresholding the image using ImageJ (NIH).

For cell migration assay, 1.2×10^5 cells were plated in duplicate into center inserts in Ibidi µ dishes and allowed to adhere for 24 h; then gaskets were removed and the distance between cell fronts from adjacent inserts were measured at the indicated times at three different spots. The migration assay was repeated once.

Blister size was measured by outlining blisters at maximum size in time-lapse images in phase movies and measuring the area in ImageJ; blister number was measured in each of seven 400×400 μm^2 fields.

Cell height was measured in ImageJ from orthogonal sections from full height *z*-stacks of WT and MRP-KO MDCK cells grown on filters for 10 days and stained for GP135 to mark the apical domain and E-cadherin to mark the extent of the lateral membrane. Cell height was measured at 12 (WT) and 18 (MRP KO) sites in multiple orthogonal sections.

Focal adhesions size and number were measured from thresholded images in ImageJ; focal adhesion number was counted in 20 cells; focal adhesion size was calculated from >2000 focal adhesions.

Non-contact frequency-modulation atomic force microscopy

MDCK cells were cultured for 10 days on a glass-bottom dish (Willco Wells). Noncontact frequency-modulation atomic force microscopy (FM-AFM) experiments were performed in duplicates on a Bruker Bioscope Catalyst AFM system (Bruker) directly mounted on an inverted Axiovert 200 M microscope (Carl Zeiss) equipped with a Confocal Laser Scanning Microscope 510 Meta (Carl Zeiss) and a 40× objective lens (0.95 NA, Plan-Apochromat; Carl Zeiss). During experiments, cells were maintained at 37°C using a heating stage (Bruker). A modified AFM microcantilever with an attached 25 µm polystyrene bead (Novascan) was used. The calibrated spring constant was 0.64 N/m (obtained using the thermal tune method built in the AFM system). Once the cells were placed on the AFM *x*-*y* stage, tapping mode was engaged. Then, the cantilever tune mode is engaged and the driving frequency selected by choosing the largest peak found near the cantilever natural frequency (Cartagena-Rivera et al., 2017). After gently engaging the monolayer surface, the cantilever tune mode was launched and the cantilever is positioned at 6 µm from the sample surface. A frequency sweep is recorded and the cantilever phase corrected to π/2. Next, the distance between the acoustically oscillating micro sphere and the monolayer apical surface, initially at 6 µm, is reduced by 500 nm intervals down to 500 nm and a frequency sweep is recorded for each interval. Epithelial tension calculations were performed using a custom-made MATLAB program (MathWorks), which is available from the corresponding author on request. The epithelial tension theory used here was recently published and can be accessed for detailed description (Cartagena-Rivera et al., 2017).

Graphs, statistics and image assembly

Graphing and statistics were performed using GraphPad Prism; analysis was by *t*-test (two groups) or one-way ANOVA followed by Tukey's multiple comparison tests (three or more groups). Image preparation was performed with ImageJ and assembly was carried out in Adobe Photoshop.

Acknowledgements

We acknowledge Robert Hogg and Aparna Kishor (National Heart, Lung, and Blood Institute, National Institutes of Health, Bethesda, MD) for use of the LightCycler 96 thermocycler, Drs Xufeng Wu, Christian Combs and Daniela Malide for help with and use of the microscopes in the NHLBI Light Microscopy Imaging Core, and Dr Christopher Bleck, Erin Stempinski and Cameron Keshavarz of the NHLBI Electron Microscopy Core. We thank Drs Vinay Swaminathan, Robert Fischer, Ana Pasapera and Karin Fredriksson for helpful discussions.

Competing interests

The authors declare no competing or financial interests.

Author contributions

Conceptualization: C.M.V.I., J.M.A.; Methodology: C.M.V.I., A.A., M.G., A.X.C.-R.; Investigation: C.M.V.I., A.J.T., A.X.C.-R.; Data curation: A.A.; Writing - original draft: C.M.V.I.; Writing - review & editing: J.M.A.; Supervision: M.G., R.S.C., J.M.A.

Funding

This research was supported by the National Institutes of Health (ZIA HL006207) to J.M.A. Deposited in PMC for release after 12 months.

Supplementary information

Supplementary information available online at
http://jcs.biologists.org/lookup/doi/10.1242/jcs.210237.supplemental

References

Anderson, J. M., Stevenson, B. R., Jesaitis, L. A., Goodenough, D. A. and Mooseker, M. S. (1988). Characterization of ZO-1, a protein component of the tight junction from mouse liver and Madin-Darby canine kidney cells. *J. Cell Biol.* **106**, 1141-1149.

Bauer, D. E., Canver, M. C. and Orkin, S. H. (2015). Generation of genomic deletions in mammalian cell lines via CRISPR/Cas9. *J. Vis. Exp.* **95**, e52118.

Bianchi-Smiraglia, A., Kunnev, D., Limoge, M., Lee, A., Beckerle, M. C. and Bakin, A. V. (2013). Integrin-beta5 and zyxin mediate formation of ventral stress fibers in response to transforming growth factor beta. *Cell Cycle* **12**, 3377-3389.

Bjerke, M. A., Dzamba, B. J., Wang, C. and DeSimone, D. W. (2014). FAK is required for tension-dependent organization of collective cell movements in Xenopus mesendoderm. *Dev. Biol.* **394**, 340-356.

Bjorkblom, B., Padzik, A., Mohammad, H., Westerlund, N., Komulainen, E., Hollos, P., Parviainen, L., Papageorgiou, A. C., Iljin, K., Kallioniemi, O. et al. (2012). c-Jun N-terminal kinase phosphorylation of MARCKSL1 determines actin stability and migration in neurons and in cancer cells. *Mol. Cell. Biol.* **32**, 3513-3526.

Blackshear, P. J., Verghese, G. M., Johnson, J. D., Haupt, D. M. and Stumpo, D. J. (1992). Characteristics of the F52 protein, a MARCKS homologue. *J. Biol. Chem.* **267**, 13540-13546.

Bruewer, M., Luegering, A., Kucharzik, T., Parkos, C. A., Madara, J. L., Hopkins, A. M. and Nusrat, A. (2003). Proinflammatory cytokines disrupt epithelial barrier function by apoptosis-independent mechanisms. *J. Immunol.* **171**, 6164-6172.

Canel, M., Serrels, A., Miller, D., Timpson, P., Serrels, B., Frame, M. C. and Brunton, V. G. (2010). Quantitative in vivo imaging of the effects of inhibiting integrin signaling via Src and FAK on cancer cell movement: effects on E-cadherin dynamics. *Cancer Res.* **70**, 9413-9422.

Cartagena-Rivera, A. X., Van Itallie, C. M., Anderson, J. M. and Chadwick, R. S. (2017). Apical surface supracellular mechanical properties in polarized epithelium using noninvasive acoustic force spectroscopy. *Nat. Commun.* **8**, 1030.

Cary, L. A., Chang, J. F. and Guan, J. L. (1996). Stimulation of cell migration by overexpression of focal adhesion kinase and its association with Src and Fyn. *J. Cell Sci.* **109**, 1787-1794.

Chang, Q. and Tepperman, B. L. (2001). The role of protein kinase C isozymes in TNF-alpha-induced cytotoxicity to a rat intestinal epithelial cell line. *Am. J. Physiol. Gastrointest. Liver Physiol.* **280**, G572-G583.
Chang, S., Hemmings, H. C., Jr and Aderem, A. (1996). Stimulus-dependent phosphorylation of MacMARCKS, a protein kinase C substrate, in nerve termini and PC12 cells. *J. Biol. Chem.* **271**, 1174-1178.
Choi, W., Acharya, B. R., Peyret, G., Fardin, M.-A., Mège, R. M., Ladoux, B., Yap, A. S., Fanning, A. S. and Peifer, M. (2016). Remodeling the zonula adherens in response to tension and the role of afadin in this response. *J. Cell Biol.* **213**, 243-260.
Chun, K.-R., Bae, E. M., Kim, J.-K., Suk, K. and Lee, W.-H. (2009). Suppression of the lipopolysaccharide-induced expression of MARCKS-related protein (MRP) affects transmigration in activated RAW264.7 cells. *Cell. Immunol.* **256**, 92-98.
Clayburgh, D. R., Shen, L. and Turner, J. R. (2004). A porous defense: the leaky epithelial barrier in intestinal disease. *Lab. Invest.* **84**, 282-291.
Clayburgh, D. R., Barrett, T. A., Tang, Y., Meddings, J. B., Van Eldik, L. J., Watterson, D. M., Clarke, L. L., Mrsny, R. J. and Turner, J. R. (2005). Epithelial myosin light chain kinase-dependent barrier dysfunction mediates T cell activation-induced diarrhea in vivo. *J. Clin. Invest.* **115**, 2702-2715.
Elias, J. E. and Gygi, S. P. (2010). Target-decoy search strategy for mass spectrometry-based proteomics. *Methods Mol. Biol.* **604**, 55-71.
Fanning, A. S., Van Itallie, C. M. and Anderson, J. M. (2012). Zonula occludens-1 and -2 regulate apical cell structure and the zonula adherens cytoskeleton in polarized epithelia. *Mol. Biol. Cell* **23**, 577-590.
Finlayson, A. E. and Freeman, K. W. (2009). A cell motility screen reveals role for MARCKS-related protein in adherens junction formation and tumorigenesis. *PLoS ONE* **4**, e7833.
Fredriksson, K., Van Itallie, C. M., Aponte, A., Gucek, M., Tietgens, A. J. and Anderson, J. M. (2015). Proteomic analysis of proteins surrounding occludin and claudin-4 reveals their proximity to signaling and trafficking networks. *PLoS ONE* **10**, e0117074.
Han, J., Zhang, G., Welch, E. J., Liang, Y., Fu, J., Vogel, S. M., Lowell, C. A., Du, X., Cheresh, D. A., Malik, A. B. et al. (2013). A critical role for Lyn kinase in strengthening endothelial integrity and barrier function. *Blood* **122**, 4140-4149.
Hartwig, J. H., Thelen, M., Rosen, A., Janmey, P. A., Nairn, A. C. and Aderem, A. (1992). MARCKS is an actin filament crosslinking protein regulated by protein kinase C and calcium-calmodulin. *Nature* **356**, 618-622.
Hell, S. W. (2007). Far-field optical nanoscopy. *Science* **316**, 1153-1158.
Hopkins, A. M., Walsh, S. V., Verkade, P., Boquet, P. and Nusrat, A. (2003). Constitutive activation of Rho proteins by CNF-1 influences tight junction structure and epithelial barrier function. *J. Cell Sci.* **116**, 725-742.
Hornbeck, P. V., Kornhauser, J. M., Tkachev, S., Zhang, B., Skrzypek, E., Murray, B., Latham, V. and Sullivan, M. (2012). PhosphoSitePlus: a comprehensive resource for investigating the structure and function of experimentally determined post-translational modifications in man and mouse. *Nucleic Acids Res.* **40**, D261-D270.
Huling, J. C., Pisitkun, T., Song, J. H., Yu, M.-J., Hoffert, J. D. and Knepper, M. A. (2012). Gene expression databases for kidney epithelial cells. *Am. J. Physiol. Renal. Physiol.* **302**, F401-F407.
Huveneers, S., Oldenburg, J., Spanjaard, E., van der Krogt, G., Grigoriev, I., Akhmanova, A., Rehmann, H. and de Rooij, J. (2012). Vinculin associates with endothelial VE-cadherin junctions to control force-dependent remodeling. *J. Cell Biol.* **196**, 641-652.
Hwang, S., Zimmerman, N. P., Agle, K. A., Turner, J. R., Kumar, S. N. and Dwinell, M. B. (2012). E-cadherin is critical for collective sheet migration and is regulated by the chemokine CXCL12 protein during restitution. *J. Biol. Chem.* **287**, 22227-22240.
Ivey, N. S., Renner, N. A., Moroney-Rasmussen, T., Mohan, M., Redmann, R. K., Didier, P. J., Alvarez, X., Lackner, A. A. and MacLean, A. G. (2009). Association of FAK activation with lentivirus-induced disruption of blood-brain barrier tight junction-associated ZO-1 protein organization. *J. Neurovirol.* **15**, 312-323.
Jean, C., Chen, X. L., Nam, J.-O., Tancioni, I., Uryu, S., Lawson, C., Ward, K. K., Walsh, C. T., Miller, N. L. G., Ghassemian, M. et al. (2014). Inhibition of endothelial FAK activity prevents tumor metastasis by enhancing barrier function. *J. Cell Biol.* **204**, 247-263.
Kannan, N. and Tang, V. W. (2015). Synaptopodin couples epithelial contractility to alpha-actinin-4-dependent junction maturation. *J. Cell Biol.* **211**, 407-434.
Kim, B. R., Lee, S. H., Park, M. S., Seo, S. H., Park, Y. M., Kwon, Y. J. and Rho, S. B. (2016). MARCKSL1 exhibits anti-angiogenic effects through suppression of VEGFR-2-dependent Akt/PDK-1/mTOR phosphorylation. *Oncol. Rep.* **35**, 1041-1048.
Koch, S. and Nusrat, A. (2009). Dynamic regulation of epithelial cell fate and barrier function by intercellular junctions. *Ann. N. Y. Acad. Sci.* **1165**, 220-227.
Koukouritaki, S. B., Vardaki, E. A., Papakonstanti, E. A., Lianos, E., Stournaras, C. and Emmanouel, D. S. (1999). TNF-alpha induces actin cytoskeleton reorganization in glomerular epithelial cells involving tyrosine phosphorylation of paxillin and focal adhesion kinase. *Mol. Med.* **5**, 382-392.
Leighton, J., Brada, Z., Estes, L. W. and Justh, G. (1969). Secretory activity and oncogenicity of a cell line (MDCK) derived from canine kidney. *Science* **163**, 472-473.
Li, J. and Aderem, A. (1992). MacMARCKS, a novel member of the MARCKS family of protein kinase C substrates. *Cell* **70**, 791-801.
Li, J., Zhu, Z. and Bao, Z. (1996). Role of MacMARCKS in integrin-dependent macrophage spreading and tyrosine phosphorylation of paxillin. *J. Biol. Chem.* **271**, 12985-12990.
Lie, P. P. Y., Mruk, D. D., Mok, K. W., Su, L., Lee, W. M. and Cheng, C. Y. (2012). Focal adhesion kinase-Tyr407 and -Tyr397 exhibit antagonistic effects on blood-testis barrier dynamics in the rat. *Proc. Natl. Acad. Sci. USA* **109**, 12562-12567.
Lipfert, L., Haimovich, B., Schaller, M. D., Cobb, B. S., Parsons, J. T. and Brugge, J. S. (1992). Integrin-dependent phosphorylation and activation of the protein tyrosine kinase pp125FAK in platelets. *J. Cell Biol.* **119**, 905-912.
Marchiando, A. M., Shen, L., Graham, W. V., Weber, C. R., Schwarz, B. T., Austin, J. R., II, Raleigh, D. R., Guan, Y., Watson, A. J., Montrose, M. H. et al. (2010). Caveolin-1-dependent occludin endocytosis is required for TNF-induced tight junction regulation in vivo. *J. Cell Biol.* **189**, 111-126.
Mui, K. L., Chen, C. S. and Assoian, R. K. (2016). The mechanical regulation of integrin-cadherin crosstalk organizes cells, signaling and forces. *J. Cell Sci.* **129**, 1093-1100.
Murphy, A., Sunohara, J. R., Sundaram, M., Ridgway, N. D., McMaster, C. R., Cook, H. W. and Byers, D. M. (2003). Induction of protein kinase C substrates, Myristoylated alanine-rich C kinase substrate (MARCKS) and MARCKS-related protein (MRP), by amyloid beta-protein in mouse BV-2 microglial cells. *Neurosci. Lett.* **347**, 9-12.
Myat, M. M., Chang, S., Rodriguez-Boulan, E. and Aderem, A. (1998). Identification of the basolateral targeting determinant of a peripheral membrane protein, MacMARCKS, in polarized cells. *Curr. Biol.* **8**, 677-683.
Rabito, C. A., Tchao, R., Valentich, J. and Leighton, J. (1978). Distribution and characteristics of the occluding junctions in a monolayer of a cell line (MDCK) derived from canine kidney. *J. Membr. Biol.* **43**, 351-365.
Rabito, C. A., Tchao, R., Valentich, J. and Leighton, J. (1980). Effect of cell-substratum interaction on hemicyst formation by MDCK cells. *In Vitro* **16**, 461-468.
Ran, F. A., Hsu, P. D., Wright, J., Agarwala, V., Scott, D. A. and Zhang, F. (2013). Genome engineering using the CRISPR-Cas9 system. *Nat. Protoc.* **8**, 2281-2308.
Rosé, S. D., Byers, D. M., Morash, S. C., Fedoroff, S. and Cook, H. W. (1996). Lipopolysaccharide stimulates differential expression of myristoylated protein kinase C substrates in murine microglia. *J. Neurosci. Res.* **44**, 235-242.
Roux, K. J., Kim, D. I., Raida, M. and Burke, B. (2012). A promiscuous biotin ligase fusion protein identifies proximal and interacting proteins in mammalian cells. *J. Cell Biol.* **196**, 801-810.
Schaller, M. D., Hildebrand, J. D., Shannon, J. D., Fox, J. W., Vines, R. R. and Parsons, J. T. (1994). Autophosphorylation of the focal adhesion kinase, pp125FAK, directs SH2-dependent binding of pp60src. *Mol. Cell. Biol.* **14**, 1680-1688.
Schober, M., Raghavan, S., Nikolova, M., Polak, L., Pasolli, H. A., Beggs, H. E., Reichardt, L. F. and Fuchs, E. (2007). Focal adhesion kinase modulates tension signaling to control actin and focal adhesion dynamics. *J. Cell Biol.* **176**, 667-680.
Swaminathan, V., Fischer, R. S. and Waterman, C. M. (2016). The FAK-Arp2/3 interaction promotes leading edge advance and haptosensing by coupling nascent adhesions to lamellipodia actin. *Mol. Biol. Cell* **27**, 1085-1100.
Tang, V. W. and Brieher, W. M. (2012). alpha-Actinin-4/FSGS1 is required for Arp2/3-dependent actin assembly at the adherens junction. *J. Cell Biol.* **196**, 115-130.
Underhill, D. M., Chen, J., Allen, L.-A. H. and Aderem, A. (1998). MacMARCKS is not essential for phagocytosis in macrophages. *J. Biol. Chem.* **273**, 33619-33623.
Van Itallie, C. M., Fanning, A. S., Holmes, J. and Anderson, J. M. (2010). Occludin is required for cytokine-induced regulation of tight junction barriers. *J. Cell Sci.* **123**, 2844-2852.
Van Itallie, C. M., Aponte, A., Tietgens, A. J., Gucek, M., Fredriksson, K. and Anderson, J. M. (2013). The N and C termini of ZO-1 are surrounded by distinct proteins and functional protein networks. *J. Biol. Chem.* **288**, 13775-13788.
Van Itallie, C. M., Tietgens, A. J., Aponte, A., Fredriksson, K., Fanning, A. S., Gucek, M. and Anderson, J. M. (2014). Biotin ligase tagging identifies proteins proximal to E-cadherin, including lipoma preferred partner, a regulator of epithelial cell-cell and cell-substrate adhesion. *J. Cell Sci.* **127**, 885-895.
Wang, F., Graham, W. V., Wang, Y., Witkowski, E. D., Schwarz, B. T. and Turner, J. R. (2005). Interferon-gamma and tumor necrosis factor-alpha synergize to induce intestinal epithelial barrier dysfunction by up-regulating myosin light chain kinase expression. *Am. J. Pathol.* **166**, 409-419.
Watanabe, T., Hosoya, H. and Yonemura, S. (2007). Regulation of myosin II dynamics by phosphorylation and dephosphorylation of its light chain in epithelial cells. *Mol. Biol. Cell* **18**, 605-616.
Wohnsland, F., Steinmetz, M. O., Aebi, U. and Vergeres, G. (2000). MARCKS-related protein binds to actin without significantly affecting actin polymerization or network structure. Myristoylated alanine-rich C kinase substrate. *J. Struct. Biol.* **131**, 217-224.
Wood, M. B., Rios, D. and Williams, I. R. (2016). TNF-alpha augments RANKL-dependent intestinal M cell differentiation in enteroid cultures. *Am. J. Physiol. Cell Physiol.* **311**, C498-C507.
Wu, M., Chen, D. F., Sasaoka, T. and Tonegawa, S. (1996). Neural tube defects and abnormal brain development in F52-deficient mice. *Proc. Natl. Acad. Sci. USA* **93**, 2110-2115.

Yue, L., Lu, S., Garces, J., Jin, T. and Li, J. (2000). Protein kinase C-regulated dynamitin-macrophage-enriched myristoylated alanine-rice C kinase substrate interaction is involved in macrophage cell spreading. *J. Biol. Chem.* **275**, 23948-23956.

Zhou, X. and Li, J. (2000). Macrophage-enriched myristoylated alanine-rich C kinase substrate and its phosphorylation is required for the phorbol ester-stimulated diffusion of beta 2 integrin molecules. *J. Biol. Chem.* **275**, 20217-20222.

Zolotarevsky, Y., Hecht, G., Koutsouris, A., Gonzalez, D. E., Quan, C., Tom, J., Mrsny, R. J. and Turner, J. R. (2002). A membrane-permeant peptide that inhibits MLC kinase restores barrier function in in vitro models of intestinal disease. *Gastroenterology* **123**, 163-172.